Adsorption of gaseous formaldehyde on Y zeolites and on metal-organic frameworks

Anaïs Becker, Nizami Israfilov, Elise Ehrstein, Irene Lara-Ibeas, Jean-Marc Planeix, Benoît Louis, Stéphane Le Calvé

ADSORPTION OF GASEOUS FORMALDEHYDE ON Y ZEOLITES AND ON METAL-ORGANIC FRAMEWORKS

Anaïs Becker[1], Nizami Israfilov[2,3], Elise Ehrstein[1,2], Irene Lara-Ibeas[1], Jean-Marc Planeix[3],

Benoît Louis[2,*], Stéphane Le Calvé[1,*]

[1] ICPEES – Institut de Chimie et Procédés pour l'Energie, l'Environnement et la Santé, Group of Atmospheric Physical Chemistry, UMR 7515 CNRS – Université de Strasbourg – ECPM, 25 rue Becquerel F-67087 Strasbourg cedex 2, France

[2] ICPEES – Institut de Chimie et Procédés pour l'Energie, l'Environnement et la Santé, Group of Energy and Fuels for a Sustainable Environment, UMR 7515 CNRS – Université de Strasbourg – ECPM, 25 rue Becquerel F-67087 Strasbourg cedex 2, France

[3] CMC – Chemistry of Complex Matter – Laboratory of Molecular Tectonics, UMR 7140 CNRS, Université de Strasbourg, 4 rue Blaise Pascal, F-67000 Strasbourg, France.

***** blouis@unistra.fr; Tel.: +33-3-68852766

***** slecalve@unistra.fr; Tel.: +33-3-68850368

Abstract

Formaldehyde is a known carcinogen and a major indoor air pollutant, which has led authorities to regulate its levels in the air. To reduce indoor airborne concentrations, several strategies can be adopted, namely the reduction of the emissions or the elimination of this pollutant by different depollution processes. Among them, adsorption on highly porous solid materials remains one of the most efficient processes.

This study aims to provide experimental data on formaldehyde adsorption capacity over different microporous materials at realistic levels (~164 ppb), being representative of the performance of the investigated materials in a real environment. For that purpose, gaseous

formaldehyde breakthrough experiments were performed under laboratory-controlled conditions over several porous solids, focusing on cation-exchanged zeolites and metal-organic frameworks (MOFs). These materials were fully characterized in terms of textural and structural properties.

Cu-based MOFs acted as more promising HCHO adsorbents than zeolites, exhibiting at least one order of magnitude higher adsorption capacity under realistic indoor conditions. Among MOFs, SUM-102 (Strasbourg University Material) exhibited the highest surfacic adsorption capacity (0.52 µg $_{HCHO}$ m^{-2}), yielding more than 1 kg $_{HCHO}$ adsorbed per $m^3_{sorbent}$ being superior to the zeolite family by at least one order of magnitude.

Keywords: formaldehyde, sorption, adsorption capacity, zeolites, MOFs, indoor air.

1. Introduction

Formaldehyde is considered as one of the major pollutants in indoor air [1,2]. Although it can be found in outdoor air emitted or produced by traffic [3–6] or photochemical reactions [3,5,7], it is typically found indoors due to the presence of several sources. Among these sources, a distinction can be made between continuous sources and point sources [8,9]. Continuous sources are, for example, construction materials (chipboard, OSB, laminate flooring, etc.) [10,11], decorative materials (paint, stains, etc.) [10,12,13] and furniture [5,9,10,12,13], especially those made from particleboard glued with urea-formaldehyde glue [14–17]. Point sources include all combustions (unvented paraffin stoves, candles, incense sticks, etc.) [5,6,13,18], the use of disinfectants and other cleaning products [4,19], etc. In addition, formaldehyde can be produced *in situ* by the reaction of ozone from outdoor air with terpenes emitted by wood-based materials [7,20–23].

Hence, formaldehyde is present in almost all indoor environments with concentrations typically ranging from 10 to 100 µg m^{-3} in domestic environments or up to several hundred µg m^{-3} in occupational environments [1,2,5,7]. Formaldehyde leads to adverse effects on human health, being considered as a carcinogen (group 1) by the IARC since 2006. Due to these harmful effects, French legislation regarding this pollutant in indoor air in public buildings has become stricter. According to

Decree No. 2011-1727 of December 2011, a limit value of 30 µg m^{-3} has been set for long-term exposure to formaldehyde since 2015. This value will be drastically lowered to a threshold of 10 µg m^{-3} starting from 2023 [24]. Its ubiquitous nature, its occurrence in indoor environments and its impact on human health make formaldehyde of great societal and scientific interest [8,18,25–28]. Scientists are continuing to develop measurement methods for this pollutant and in particular real-time instruments such as analysers [29–36] and sensors [37–42] for monitoring indoor air. In addition, low cost indoor air quality measurement devices are now available for individuals willing to improve the quality of the air they breathe [43,44].

Adsorption techniques are widely used for air pollution control [45–47] and sampling of pollutants before desorption and analysis by off-line or on-line methods [29–31,33,34,48,49]. However, the efficiency of common adsorbents towards the formaldehyde molecule is limited due to its high polarity and small size. In this context, many studies have focused on the characterisation of formaldehyde adsorption over a wide variety of materials commercially available as well as synthesised in research institutes [50–57] (see **Table 1**).

Formaldehyde adsorption studies under perfectly controlled conditions involve firstly the generation of known concentrations of gaseous formaldehyde. Gaseous formaldehyde is rarely available in gas cylinders and must therefore be generated *in situ* from calibrated permeation tubes [58–61] or aqueous formaldehyde solutions [59,61–63]. Both generation systems need to be regulated in temperature and gas flow rate to ensure a stable concentration. A second difficulty relies on the measurement of formaldehyde in the gas phase by means of a high-performance analytical instrument able to monitor the concentration in real time. Although several analytical methods are reported in the literature, most of them [29–36], including sensors [37–42], are only reliable to measure high concentrations because of their limited sensitivity. Due to these aforementioned technical constraints, most of the studies have been carried out at high formaldehyde concentrations (1 to 150 ppm) [50–54] which are not representative of the concentrations encountered in indoor environments. In contrast, our research institute has carried out studies using ~164 ppb formaldehyde concentration [56]. For the same adsorbent material, working at a lower concentration of gaseous formaldehyde implies a longer

time to reach the saturation during the adsorption experiment and therefore a very stable gas generation over periods typically varying from a few hours to roughly ten days, depending on the adsorption capacity of the material. All these constraints and technical difficulties justify the scarce data obtained at realistic concentrations of gaseous formaldehyde as illustrated in **Table 1**.

Table 1. Formaldehyde adsorption capacities achieved over different porous materials and various formaldehyde concentrations

Adsorbent	Adsorbent Type	S_{BET} (m^2 g^{-1})	Pore size (nm)	Concentration (ppm)	Adsorption Capacity (mg g^{-1} ads)	Reference
HKUST-1	MOF	1,733	0.54 / 0.69	0.164	0.504	Lara-Ibeas *et al.*, 2020
CBV3020E - Mg	Zeolite	296	0.55	0.164	0.035	Lara-Ibeas *et al.*, 2020
AC	AC	942	n. a.	10	2	Bellat *et al.*, 2015
SBA-16	MS	572	3.4 / 6.0	0.164	0.029	Lara-Ibeas *et al.*, 2020
CBV3020E	Zeolite	369	0.55	0.164	0.026	Lara-Ibeas *et al.*, 2020
ZSM-5_79	Zeolite	348	0.55	0.164	0.022	Lara-Ibeas *et al.*, 2020
ZSM-5_132	Zeolite	352	0.55	0.164	0.015	Lara-Ibeas *et al.*, 2020
ZSM-5_198	Zeolite	367	0.55	0.164	0.01	Lara-Ibeas *et al.*, 2020
Ag/HZSM-5	Zeolite	310	0.55	29.7	0.77	Zhao *et al.*, 2015
Carbopack® B	AC	112	-	0.164	0.004	Lara-Ibeas *et al.*, 2020
MIL-53 (Ga)	MOF	560	n. a.	10	0.2	Bellat *et al.*, 2015
Cu/HZSM-5	Zeolite	314	n. a.	29.6	0.49	Zhao *et al.*, 2015
HZSM-5 (SAR = 360)	Zeolite	n. a.	n. a.	24.4	0.35	Zhao *et al.*, 2015

AC: activated carbon; MS: mesoporous silica

However, the adsorption capacity depends strongly on the partial pressure of the gas. At low concentrations, the adsorption capacity increases linearly with the partial pressure in accordance with the Langmuir model [64,65], which potentially allows the extrapolation of the experimental data to other gas concentrations. Conversely, at higher concentrations, this relationship is no longer linear, which prohibits any extrapolation to lower concentration values. Lara-Ibeas (2020) [56] gathered experimental data regarding adsorption studies of gaseous formaldehyde over different materials

(Figure 7 in [56]). This figure highlights a clear lack of existing experimental data in the literature on the adsorption of formaldehyde at concentrations in the range of tens to hundreds of ppb.

Since adsorbents need to possess a high specific surface area (SSA) to reach high adsorption capacities, zeolites and metal-organic frameworks are often selected. Indeed, the presence of numerous micropores increases the surface area per volume, rendering these highly microporous solids efficient and hence a suitable choice.

Herein, formaldehyde adsorption was investigated over a series of cationic-exchanged FAU zeolites and as-synthesized SUM (Strasbourg University Materials) metal-organic frameworks (MOFs) at ppb levels. This allowed the evaluation of the effect of the cation nature, present in the zeolite as charge compensation, as well as the nature of the porous sorbent on the adsorption performance.

The main objective of this study is therefore to provide accurate and quantitative information on the adsorption performance of a range of materials at realistic formaldehyde concentrations, using an experimental device combining a stable source of gaseous formaldehyde and a formaldehyde analyser developed in our laboratory.

2. Materials and methods

2.1. Adsorbents

2.1.1 Cation-exchanged zeolites

Commercially available HUSY (Zeoflair 200, Zeochem, Uetikon, Switzerland) was used as received for performing adsorption tests. In order to prepare cation-exchanged faujasite (FAU) zeolites, $CuCl_2.2H_2O$ (Alfa Aesar, 97%), $Ca(NO_3)_2.4H_2O$ (Prolabo, 99%), $Zn(NO_3)_2.6H_2O$ (Sigma Aldrich, 99%) and Ag_2SO_4 (Prolabo, 99%) were used without any purification step. All cationic exchanged zeolites were prepared according to the following protocol inspired by Maia *et al.* [66]: 3g of HUSY zeolite was dispersed in 100 mL of distilled water in a 250 mL round-bottomed flask and

stirred vigorously. Then, the appropriate amount of metal salt (between 1-5 wt.% nominal value) was added to the mixture and stirred at 70 °C for 2 h. After, the solution was dried in a rotavapor at 50 °C under vacuum until complete removal of water. Finally, the solid was dried at 110 °C overnight and calcined at 550 °C for 5 h (ramp 1°C min^{-1}). A white powder is obtained in the cases of Ca-, Zn- and Ag-USY zeolites, whilst Cu-USY exhibited its classical blue color.

2.1.2 Metal-organic frameworks

HKUST-1 (Basolite® C300, Sigma-Aldrich) was used as received as a benchmark adsorbent. Polyethylene glycol modified terphenyl tetracarboxylate ligands were used for the preparation of copper-based MOFs: SUM-102 and SUM-103 materials [67]. The MOF named herein as Cu@H4L1, also called UTSA-90 was first synthetised by Zhou *et al.* [68]. Detailed synthesis protocols SUM-102 (glyme), or Cu@H4L2, and SUM-103 (diglyme), or Cu@H4L3, can be found in a former publication [67]. **Figure 1** presents the chemical structure of the different ligands used to generate their associated Cu MOFs.

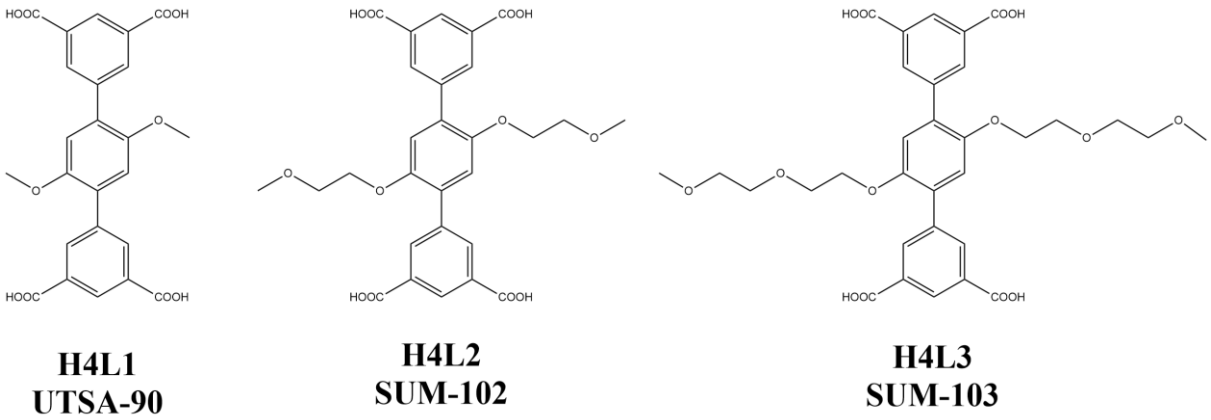

Figure 1. Ligands used to generate corresponding Cu-based MOFs

2.2. Characterization

X-ray diffraction patterns were recorded on a Bruker D8 Advance diffractometer, with a Ni detector side filtered Cu Kα radiation (1.5406 Å) over a 2θ range of 5-60° for zeolites and 4-40° for

MOFs. Scanning electron microscopy (SEM) images were acquired in a ZEISS GEMINI SEM 500 microscope using an electron high tension (EHT) voltage ranging from 2 to 6 kV. To determine the elemental distribution, EDX and mapping analyses were also performed using an EDAX SDD detector.

Nitrogen adsorption-desorption isotherms for all zeolites were recorded at 77 K using a Micromeritics ASAP 2420, while ASAP 2050 equipment was used for all MOFs. The specific surface area and pore volume were calculated using the Brunauer–Emmett–Teller (BET) method. Prior to analysis, MOF samples were pre-treated *in-situ* at 180°C for 5 h under vacuum. Zeolites were pre-treated at 250°C under vacuum during 10 h.

2.3. Formaldehyde monitoring and adsorption

Formaldehyde was monitored on-line using a patented and marketed device initially developed in our institute and detailed in previous studies [31,69,70]. Briefly, this analytical method is based on three highly coupled steps: i) uptake of gaseous formaldehyde into an aqueous acetylacetone solution at room temperature (gas and liquid flow rates set to 20 mL min^{-1} and 17 µL min^{-1}, respectively); ii) chemical reaction between formaldehyde and acetylacetone at 65°C *via* the Hantzsch reaction [71]; and iii) *on-line* fluorescence detection of the reaction product, *i.e.*, 3.5-diacetyl-1.4-dihydrolutidine (DDL), excited by a LED centered at 415 nm and fluorescence collected on a photomultiplier (Hamamatsu) coupled to a 530 ± 40 nm band pass filter. The commercial formaldehyde analyser (microF, Chromatotec, Val-de-Virvée, France) has a temporal resolution of 2 s, a response time of 10 min and a detection limit of about 1 µg m^{-3} (0.81 ppb). These data can be averaged to obtain time steps typically varying between 10 min and 1 hour [12]. In this work, zeolite and MOF data were averaged over 1-5 and 20 minutes, respectively.

Each investigated material was introduced separately in a copper tube (1/8-inch outer diameter) where it was packed between two quartz wool plugs. The exact amount of adsorbent was weighted with a precision balance, with an error of 0.2 mg. This tube was then mounted in the experimental setup shown in **Figure 2**. To ensure a constant gaseous formaldehyde concentration of

164 ppb, a synthetic air flow (10 mL min^{-1}) was passed through a formaldehyde aqueous solution (0.0925 wt.%) maintained at 20°C thanks to a Peltier modulus and then diluted in a second synthetic air flow (390 mL min^{-1}). A resulting formaldehyde gaseous flow of 164 ppb could therefore be generated [31,33,69]. The resulting overall relative uncertainty of the pre-calibrated and generated gaseous concentration was calculated to be in the range of 9-11%. Before the adsorption experiments, the gas was flown through the bypass, diluted and analysed. The obtained intensity corresponds to the initial concentration (C_0) and, therefore, it was used as an indicator to determine when saturation was reached, *i.e.*, when the outlet concentration was equal to the inlet concentration ($C = C_0$). All the adsorption experiments were performed at room temperature, i.e., 20 ± 3 °C.

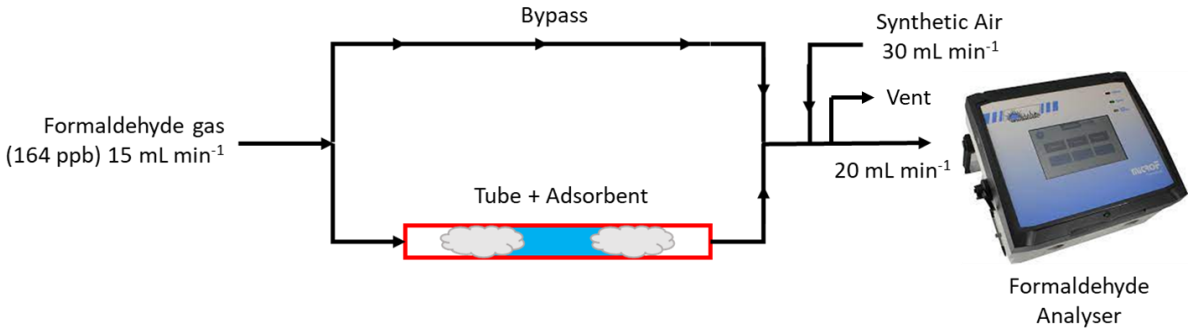

Figure 2. Scheme of the experimental set-up

3. Results and discussion

3.1. Samples characterisation

3.1.1 Zeolites

Pristine and cationic exchanged-FAU zeolites were characterised to assess their metal loading, their textural and their structural properties. summarizes these data along with the adsorption capacity of formaldehyde and breakthrough time which will be deeper discussed in **Section 3.2.** It is worthy to mention that all exchanged zeolites (Cu^{2+}, Zn^{2+}, Ag^{+} and Ca^{2+}) exhibit similar pore volumes and BET surface areas, thus enabling the evaluation of metal nature and loading effects. Indeed, a limited

decrease to 15% both in BET area and pore volume values could be observed in the highest loaded 3Ag-HUSY zeolite. Likewise, the crystalline structure integrity was preserved after the cationic exchange step as shown in **Figure 3**. Besides, the loading of the different cations within the FAU structure corresponds to the amount introduced in the aqueous solution, in line with our former studies [56,57].

Table 2. Textural and adsorption properties of the exchanged FAU zeolites

Adsorbent	**Cation loading [% wt.]**	**SSA values [m^2 g^{-1}]**	**Pore volume [cm^3 g^{-1}]**	**Mass [mg]**	**Adsorption capacity [µg g^{-1}]**	**Breakthrough time [min]**	**Saturation time [min]**
HUSY	0	644	0.43	6.3	14.0 ± 1.6	2	95
Cu1-HUSY	0.9	568	0.36	5.3	37.4 ± 4.2	15	220
Cu3-HUSY	3.0	569	0.36	6.5	20.9 ± 2.9	2	85
Ag1-HUSY	1.0	662	0.43	4.2	20.3 ± 2.8	1	100
Ag3-HUSY	2.1	549	0.37	3.4	22.5 ± 0.8	5	125
Ca3-HUSY	3.4	594	0.37	3.6	21.4 ± 3.1	3	100
Zn3-HUSY	4.1	644	0.42	5.3	34.1± 0.5	5	210

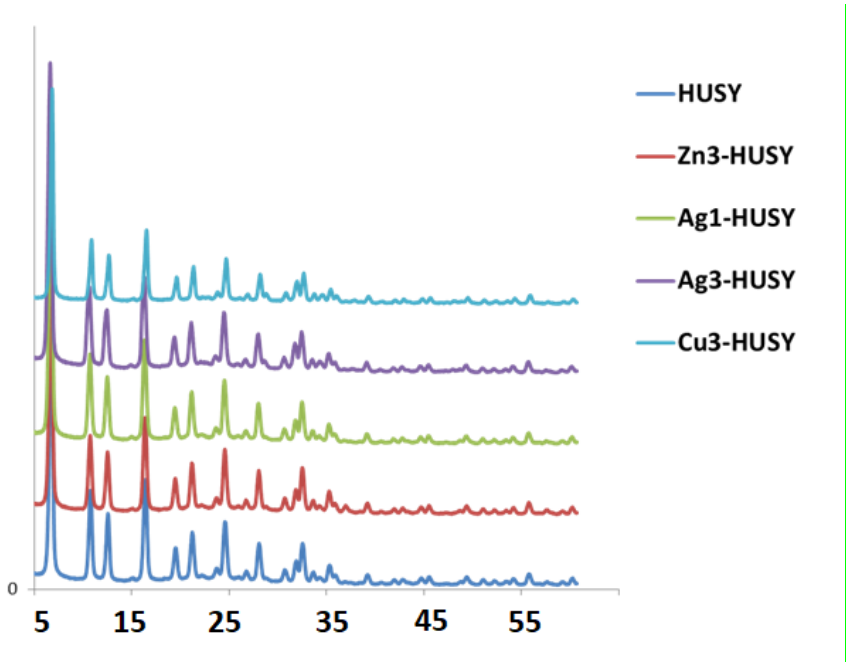

Figure 3. XRD patterns of pristine and cation-exchanged FAU zeolites

3.1.2 MOFs

The textural properties of Cu-based MOFs were evaluated by N_2 adsorption-desorption at -196°C, showing classical Type I isotherms **(**see **Fig. S1)**. **Table 3** presents the specific surface area values as well as their pore volumes. In contrast to benchmark HKUST-1 material, SUM-102 and SUM-103 exhibit both lower SSA and pore volume values which may negatively impact their adsorption capacity.

The structure of the different MOFs was evaluated by powder XRD (**Figure 4)**. It is important to highlight that both SUM-102 and SUM-103 materials exhibit the same topology and connectivity mode of tetracarboxylate ligands as pristine NOTT-101 [72]. The presence of either glyme (SUM-102) or diglyme (SUM-103), as lateral chains of tetracarboxylate ligands (**Figure 1**), did not alter the MOF structure integrity.

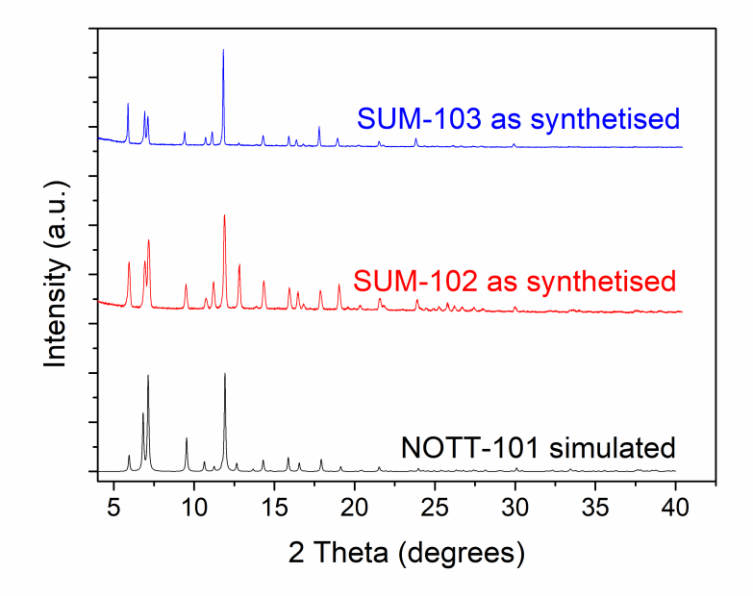

Figure 4. XRD patterns of NOTT-101, SUM-102 and SUM-103 materials

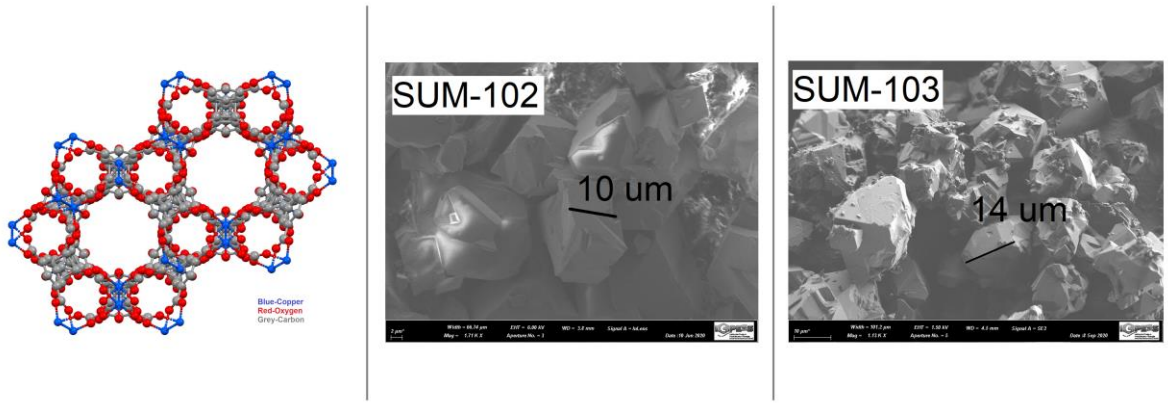

(a) (b) (c)

Figure 5. (a) view from c axis of NOTT-101, (b) SEM image of SUM-102 and (c) SUM103.

Figure 5a shows the pore aperture of MOFs, solved from a single crystal diffraction study of NOTT-101, (without the presence of glyme side chains). However, it has been shown that the presence of those chains led to a drastic improvement in the stability in water ranging from NOTT-101 up to SUM-103 [67]. According to SEM micrographs, crystals in the range of 10-20 µm could be observed (**Figure 5b et 5c**).

3.2. Evaluation of formaldehyde adsorption capacity

3.2.1 Calculations

Dynamic adsorption experiments were performed to obtain the corresponding breakthrough curves representing the evolution of the adsorbate concentration in the effluent leaving the adsorbent bed as a function of time. In air treatment, the breakthrough time is usually defined as the time in which 5% of the feed concentration (C_0) is leaving the adsorbent bed. Additionally, breakthrough curves allow determining the total adsorption capacity of each material. This capacity can be calculated from each curve using equation (1):

$$q = \frac{Q\ C_0}{\mathrm{m}} \int_{t_0}^{t_s} \left(1 - \frac{C}{C_0}\right) dt \qquad (1)$$

where q represents the dynamic adsorption capacity per gram of adsorbent, Q is the gas flow rate, m is the mass of adsorbent, t_0 corresponds to the initial time and t_s to the saturation time, C_0 is the initial concentration, and C is the outlet concentration at a given time.

The error on the calculation of the dynamic adsorption capacity was estimated according to Eq.2 :

$$\frac{\Delta q}{q} = \frac{\Delta Q}{Q} + \frac{\Delta C_0}{C_0} + \frac{\Delta t}{t} + \frac{\Delta m}{m} \qquad (2)$$

where Δq is the error on the adsorption capacity. ΔQ is the error on the flow rate, ΔC_0 is the error on the initial concentration and Δm is the error on the adsorbent mass.

3.2.2 Zeolites

Preliminary experiments were performed by varying the mass of pristine HUSY and Cu-USY (loading 1% in weight) in the reactor set-up (**Figure 6a**). Since the adsorption capacities did not vary significantly and to maintain the pressure drop in the reactor acceptable, the value of 3 mg was set arbitrarily to compare all adsorbents.

It is important to highlight here that whatever the nature of the cation exchanging the proton in the FAU structure, a higher adsorption capacity was achieved. **Figure 6b** shows the results obtained with 3% wt. of the different elements. Adsorption capacities were assessed by numerical integration of the area above the breakthrough curve and are also presented in **Figure 6**. The best performance was achieved by Zn3-HUSY which exhibited a 2.5 higher adsorption capacity with respect to pristine HUSY, i.e., 34 versus 14 µg / $g_{zeolite}$. Likewise, the breakthrough time increased from 2 to 5 min over the former Zn-loaded zeolite (**Table 2**). To evaluate the kinetics of formaldehyde adsorption, it is important to compare the profile of those breakthrough curves. The adsorption of formaldehyde was complete during the first minutes (**Figure 7a**). The shape of the obtained breakthrough curves remained similar in all cases (**Figure 7a**). A focus on the first 20 min of the adsorption test is displayed in **Figure 7b**.

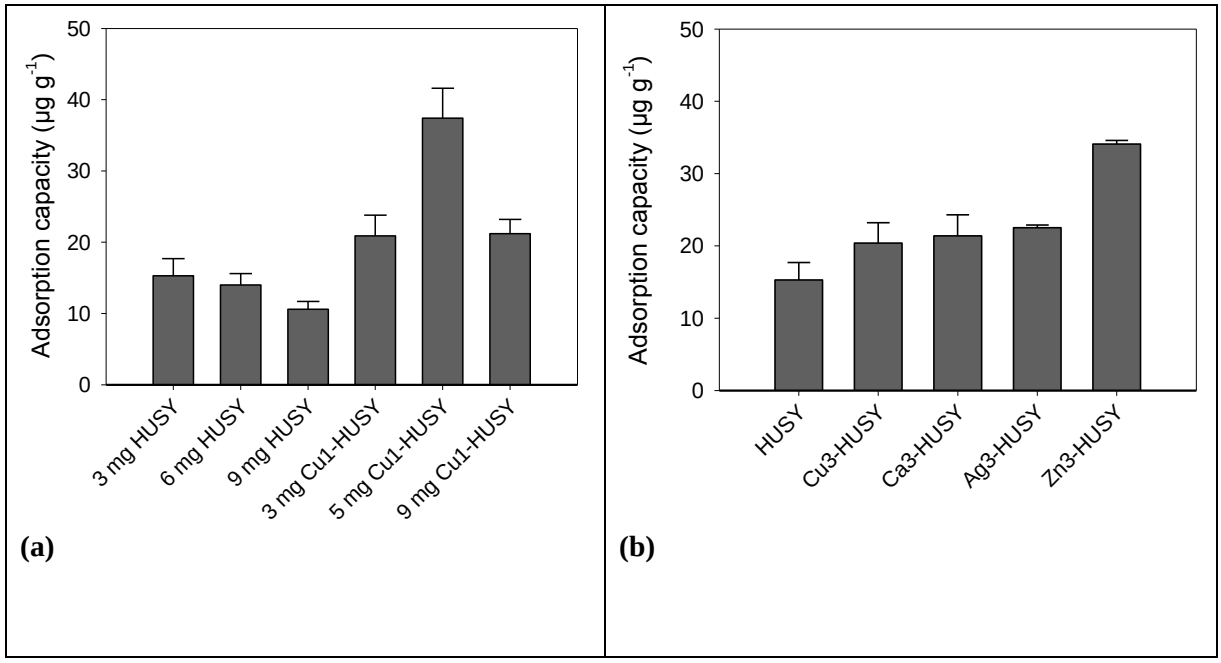

Figure 6. Adsorption capacity **(a)** by varying the mass of adsorbent **(b)** by varying the nature of the cation in the zeolite.

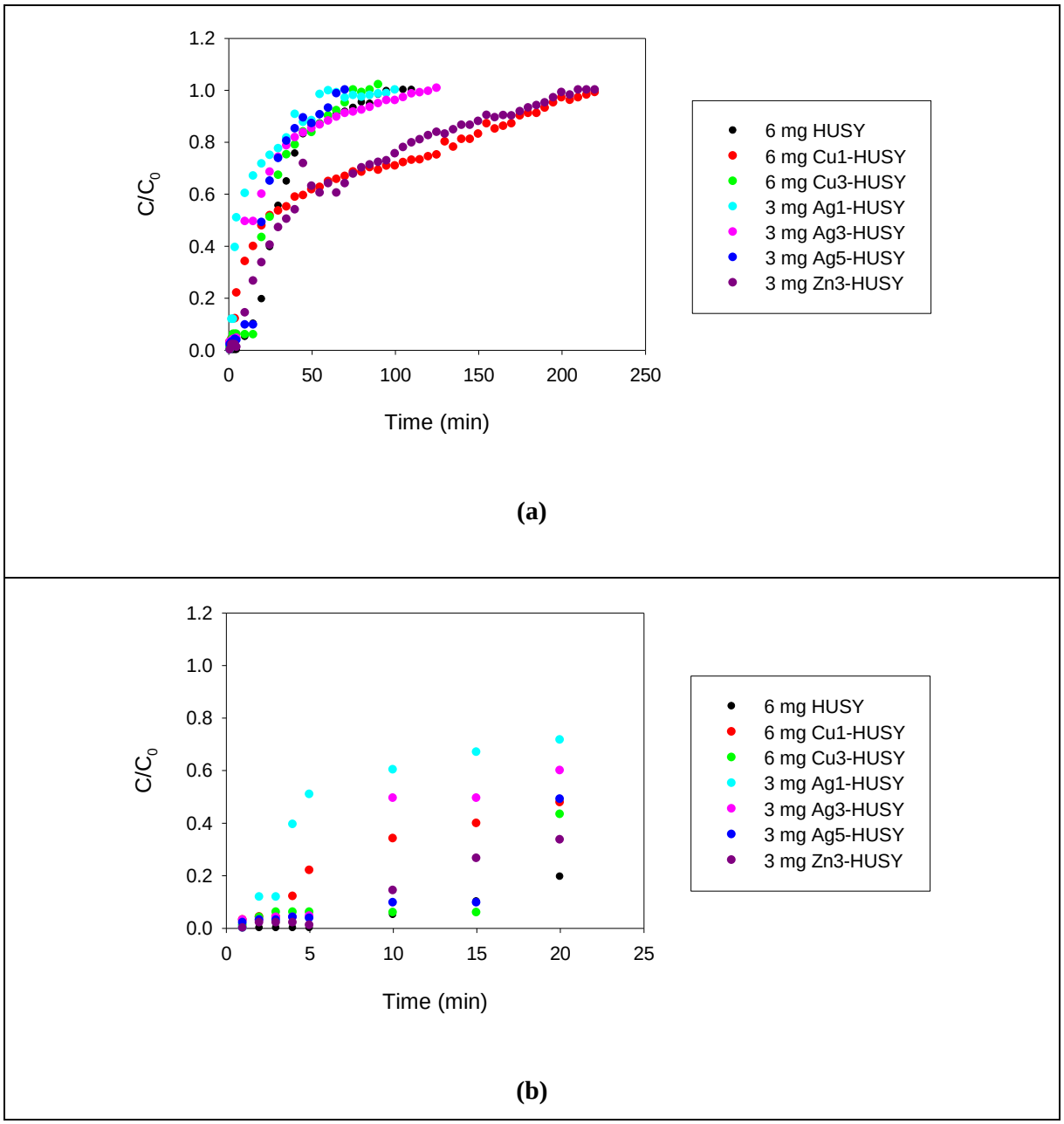

Figure 7. Breakthrough curves at room temperature and at 164 ppb of formaldehyde **(a)** for different metal-exchanged zeolites **(b)** zoom on the first 20 min of the adsorption test (formaldehyde concentration = 164 ppb, flow rate = 15 mL min^{-1}).

The breakthrough points of formaldehyde adsorption reached 2, 5 and 15 min for HUSY, Zn3-HUSY and Cu1-HUSY, respectively. After the breakthrough point, two different slopes can be distinguished thus providing information regarding a different kinetic behavior. At first, a sharp increase in the outlet concentration is observed which indicates fast kinetics followed by a continuous

but slow increment of the concentration until the initial concentration was reached, suggesting that the adsorption kinetics close to the adsorbent saturation becomes much slower.

The results obtained in the present contribution are in line with our former study dealing with MFI-type zeolite [57]. Indeed, breakthrough times were also observed to be in the same range of 4-7 min over H-ZSM-5 and Mg-doped ZSM-5, respectively. In addition, the same trend could be confirmed herein that an exchange of a proton by another cation led to an enhanced adsorption capacity.

The less efficient sorbent remained the HUSY zeolite in which full saturation was reached in less than one hour. This behaviour might be related to the surface chemistry, minimising adsorbate-adsorbent interactions. The latter should therefore solely rely on London forces or limited interactions with the zeolite bridged hydroxyl groups. It is therefore beneficial to exchange protons by other extra-framework cations to modulate those adsorbate-adsorbent interactions [73,74]. Recently, Megías-Sayago *et al.* demonstrated a 30% adsorption capacity increase while partially exchanging zeolite protons by Mg^{2+} cations under similar conditions [57]. Though the adsorption of formaldehyde molecules was shown to be directly related to the Al content, thus to the amount of Brønsted acid sites in zeolites [75], the adsorption process seems to be ruled by the interactions between the carbonyl group and the zeolite counter cation.

The enhancement in the adsorption capacity, observed over all cation-exchanged FAU zeolites, suggests that formaldehyde established stronger interactions with Ca^{2+}, Cu^{2+}, $Zn^{2+,}$ Ag^{+} than with H^{+}, in line with the observations from Bellat *et al.* [50,76].

Such order of enhanced interaction with Ag^{+} or Cu^{2+} may be related to the Hard-Soft Acid and Bases (HSAB) theory developed by Pearson in 1963 [77]. Indeed, soft cations such as silver, copper and to less extent zinc, demonstrate a higher affinity towards a relatively soft base as the HCHO molecule [78,79]. Kleiber *et al.* have shown that the metal ion-aldehyde interaction generally occurs in an end-on M^{+} - OCRH configuration [80]. These considerations may explain, at least partially, the longer breakthrough times observed over Ag-, Cu- and Zn-HUSY.

From those adsorption experiments with metal-doped zeolites, it appears that the rational design of efficient formaldehyde adsorbents needs to combine both high microporosity and (soft) Lewis acid content. We have therefore selected Cu-based MOFs as potential candidates to fulfil these two necessary conditions.

3.2.3 MOFs

Breakthrough curves for the different Cu-MOFs are presented in Figure 8.

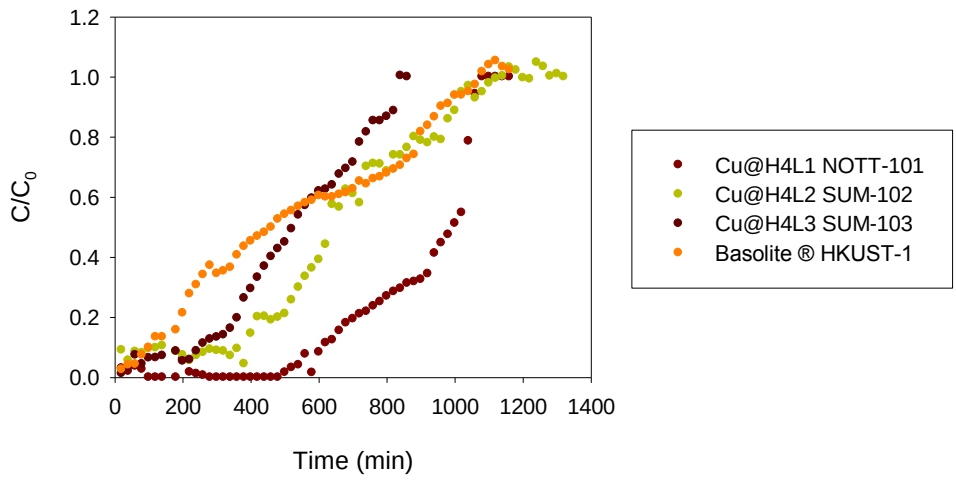

Figure 8. Breakthrough curves for the different Cu-based MOFs at room temperature and at 164 ppb of formaldehyde

It is worthy to highlight here that Cu@H4L1 material exhibited an exponential adsorption behavior. In stark contrast, SUM-102 and SUM-103 showed a similar stepwise adsorption phenomenon. HKUST-1 led also to stepwise HCHO adsorption but less pronounced (**Figure 8**). The stepwise desorption of formaldehyde indicates the presence of different active sites in the SUM series, which induced a slower release with respect to Cu@H4L1. This indicates that the presence of side chains on L2 and L3 ligands (**Figure 1**) induced a different adsorption behavior than pristine UTSA-

90 material. It appears however that the necessary time to reach saturation is almost the same (as shown in **Table 3**).

Table 3. Textural properties of MOFs and their HCHO adsorption capacity data

Adsorbent	**SSA values [m^2 g^{-1}]**	**Pore volume [cm^3 g^{-1}]**	**Mass [mg]**	**Adsorption capacity [µg g^{-1}]**	**Breakthrough time [min]**	**Saturation time [min]**	**HCHO surfacic adsorption capacity [µg m^{-2}]**	**HCHO volumetric adsorption capacity [g m^{-3}]**
Basolite®C 300 **HKUST-1**	1733	0.89	3.0	504 ± 87	70	1040	0.29	566
Cu@H4L1 UTSA-90	1239	0.63	5.2	513 ± 58	490	1152	0.41	814
Cu@H4L2 SUM-102	870	0.45	5.6	453 ± 50	10	1110	0.52	1007
Cu@H4L3 SUM-103	1058	0.57	6.5	302 ± 33	60	834	0.29	530

HKUST-1 has been shown to achieve the highest HCHO adsorption performance among benchmark adsorbents [57,81]. This remarkable capacity can be explained by several factors: i) a high specific surface area that provides numerous adsorption sites; ii) micropores with diameters of 5.4 and 6.9 Å suitable for formaldehyde adsorption (kinetic diameter = 2.5 Å); iii) a coordination bond between the copper atoms and the O-atom from the carbonyl group.

Table 3 shows the SSA values and pore volumes of HKUST-1 benchmark adsorbent and homemade SUM family of Cu-MOFs. The former commercial material exhibited the highest SSA (1733 m^2 g^{-1}) and pore volume (0.89 cm^3 g^{-1}) with respect to as-prepared MOFs, corresponding to the double of those from SUM-102. As *'a priori'* expected, HKUST-1 led to a high adsorption capacity of

504 µg g^{-1} (see **Table 3**). However, Cu@H4L1 (UTSA-90) led roughly to the same result (513 µg g^{-1}) despite its 30% lower SSA value. According to the normalization of the adsorption capacity per surface and volumetric unit (**Table 3**), it is important to highlight that SUM-102 outperformed both UTSA-90 and HKUST-1 with an adsorption of 0.52 µg $_{HCHO}$ m^{-2} and 1007 g $_{HCHO}$ m^{-3}. A further increase in the side chain length of the ligand (**Figure 1**), ranging from Cu@H4L2 to Cu@H4L3, led to a drastic decrease in the sorption performances (**Table 3**). SUM-102 seems therefore to be a proper compromise in terms of pore size (~ 9-10 Å) and interactions provided with HCHO molecules. The longer chain length found in the H4L3 ligand which built SUM-103 led to a drastic decrease in the MOF porosity and SSA value, thus probably to formaldehyde molecules' accessibility. It is however important to highlight that SUM-103 led to nearly the same surfacic and volumetric adsorption capacity as HKUST-1, in spite of 60% lower SSA. Supramolecular interactions created by these glyme and diglyme moieties may probably explain this different behaviour, as suggested by Israfilov *et al.* [67].

The measurement of saturation times remains a mean to get precious insights into adsorbate-adsorbent interactions (**Table 3**). Again, extremely high values were obtained with SUM MOFs family: 1152, 1110 and 834 min for Cu@H4L1, Cu@H4L2 and Cu@H4L3, respectively. Those values are in line with the one obtained with HKUST-1 (1040 min). In stark contrast, the breakthrough time reached only limited values for HKUST-1 (70 min) and SUM materials (10 and 60 min, respectively for SUM-102 and SUM-103) with respect to Cu@H4L1 which demonstrated a prolonged time of 490 min before releasing 5% of HCHO concentration. It seems therefore that a high affinity between HCHO molecules and Cu@H4L1 surface could be assessed. The design of SUM materials, using glyme or diglyme moieties on the ligand, probably led to specific and different modes of interaction between HCHO and those side-chains. This may induce the rapid release of a significant fraction of barely adsorbed HCHO molecules. Moreover, these side chains may hinder the accessibility and diffusion of formaldehyde inside and outside the micropores. Indeed, the stepwise desorption observed over SUM-102 and SUM-103 could be tentatively explained by such a phenomenon. The pore size decrease from 10.9 to 9.8 and 9.2 Å, ranging from Cu@H4L1 to Cu@H4L3 is certainly due to a lower accessibility of N_2 molecules in the MOF internal porosity.

Despite HKUST-1 exhibiting a high adsorption capacity (compared with zeolites), it is therefore important to point out that the rational design of NOTT MOFs, led to further enhancing breakthrough time (Cu@H4L1) and volumetric adsorption capacity (Cu@H4L2, SUM-102).

Finally, a significant decrease in formaldehyde adsorption capacity is usually observed over HKUST-1 in humid environments due to its hydrophilic character, hence leading to a significant loss in stability [55,82]. In contrast, the amphiphilic character of the pores introduced by the ethylene glycol chains in SUM materials gave birth to specific stability in water, thus to a strong potential for use in a humid atmosphere.

3.2.4 Comparison between zeolites and MOFs

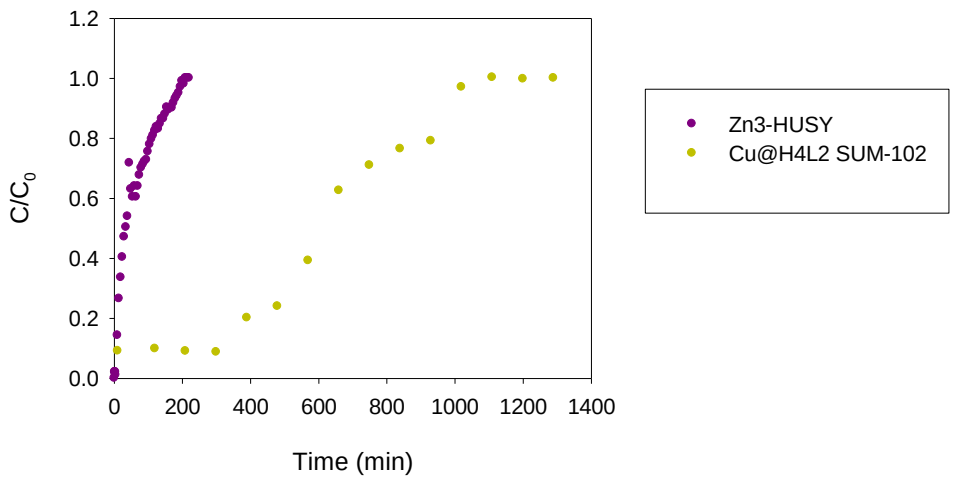

Figure 9. Breakthrough curves comparison between zeolite Zn3-HUSY (adsorption capacity of 34 µg g^{-1}) and MOF Cu@H4L2 SUM-102 (adsorption capacity of 453 µg g^{-1}), obtained at room temperature and at 164 ppb of formaldehyde

Figure 9 shows a clear comparison of breakthrough curves for representative Zn3-HUSY zeolite and SUM-102 MOF which highlights both a much higher adsorption capacity and saturation

time over MOFs. Finally, this tendency could be confirmed for all-tested adsorbents as shown in **Figure 10**.

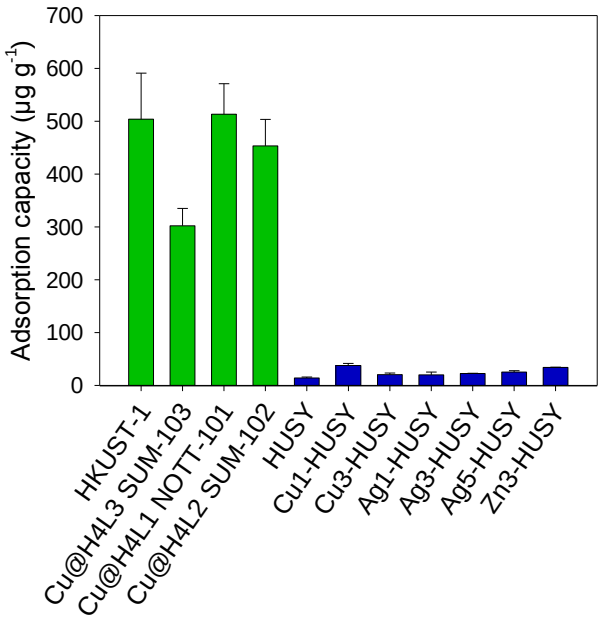

Figure 10. Adsorption capacity comparison between MOFs in green and Zeolites in blue, obtained at room temperature and at 164 ppb of formaldehyde.

Motivated by its occurrence in indoor air and the underlying harmful effects, formaldehyde adsorption has been studied over porous solids such as metal-promoted zeolites and MOFs. As shown in **Table 1**, only a few studies were conducted at realistic formaldehyde concentrations from 0.16 to 1 ppm, being representative of ambient conditions. Herein, we achieved similar results over Cu-, Zn-, Ca- and Ag-doped FAU zeolites (**Table 2**) to the ones obtained in the literature under such a low formaldehyde concentration. Interestingly, Metal-Organic Framework materials led to nearly one order of magnitude higher adsorption capacity, especially Cu-based MOFs. For instance, MIL-53(Ga) did not yield high performance at 10 ppm HCHO concentration (**Table 1**).

Our findings suggest that special adsorbate-adsorbent interactions could be created in Cu-based MOFs, especially in as-prepared SUM-102 and SUM-103 materials. To avoid possible misinterpretation, the Henry constant (K_H) is commonly calculated for comparison purposes instead of

adsorption capacity [83–86]. K_H (mol kg^{-1} Pa^{-1}) is a key parameter to explain the gas-solid adsorption phenomena, evaluating the adsorption affinity of a material for a certain adsorbate. K_H, calculated according to **Eq. 3**, can only be considered valid at relatively low pressures (< 100 Pa corresponding to ~1,094 ppm), where it is assumed that the adsorption capacity raises linearly with the adsorbate partial pressure [85].

$$K_H = \frac{q}{P_f \, M_f} \tag{3}$$

where q (kg kg^{-1} adsorbent) is the adsorption capacity, P_f is the formaldehyde partial pressure (Pa) and M_f is the molecular weight of formaldehyde (kg mol^{-1}).

The K_H values obtained for the M-HUSY zeolite series ranged from 0.03, for pristine HUSY, up to 0.10 mol kg^{-1} Pa^{-1} for Ag-HUSY (0.08 mol kg^{-1} Pa^{-1} for Cu-HUSY). Similar values were calculated by Bellat *et al.* for NaY zeolite (K_H = 0.13 mol kg^{-1} Pa^{-1}) thus confirming that surface chemistry, *i.e.*, adsorbate-adsorbent interactions might govern the adsorption of formaldehyde [76]. Moreover, K_H values lower than 0.1 mol kg^{-1} Pa^{-1} are generally characteristic of weak adsorbate-adsorbent interactions [87].

Regarding Cu@H4L1, Cu@H4L2 and Cu@H4L3, Henry constant values, K_H = 1.14; 1.01; 0.67 mol kg^{-1} Pa^{-1} were obtained, respectively. This confirms a decreasing affinity between formaldehyde and the NOTT- MOF surfaces, being in line with decreasing breakthrough times. Surprisingly, HKUST-1 led to K_H = 1.12 mol kg^{-1} Pa^{-1} which indicates a high affinity between HCHO and the surface, without a sufficient breakthrough time. Further studies need to be performed to understand the behaviour and also try to further improve those values, possibly by following the approach undertaken by Fu et *al.* which yielded an 8-12 higher adsorption capacity while shifting from ZIF-8 to Ag@ZIF-8 [88].

Hence, adsorbents showing K_H values from 0.1 to 1.2 mol kg^{-1} Pa^{-1} exhibit a non-negligible formaldehyde adsorption capacity, being suitable for pollutant removal and enabling a quantitative

sampling for gas analysis applications. Furthermore, the intermediate strength of the interactions may presumably lead to milder conditions for desorption and are therefore expected to be more appropriate.

Finally, higher formaldehyde adsorption capacity was achieved at low concentration, rendering SUM-102 material (mainly) a potential candidate for pollutant removal purposes in real atmospheric conditions. Consequently, its use in humid environments seems possible and should avoid an upstream device for water trapping.

4. Conclusions

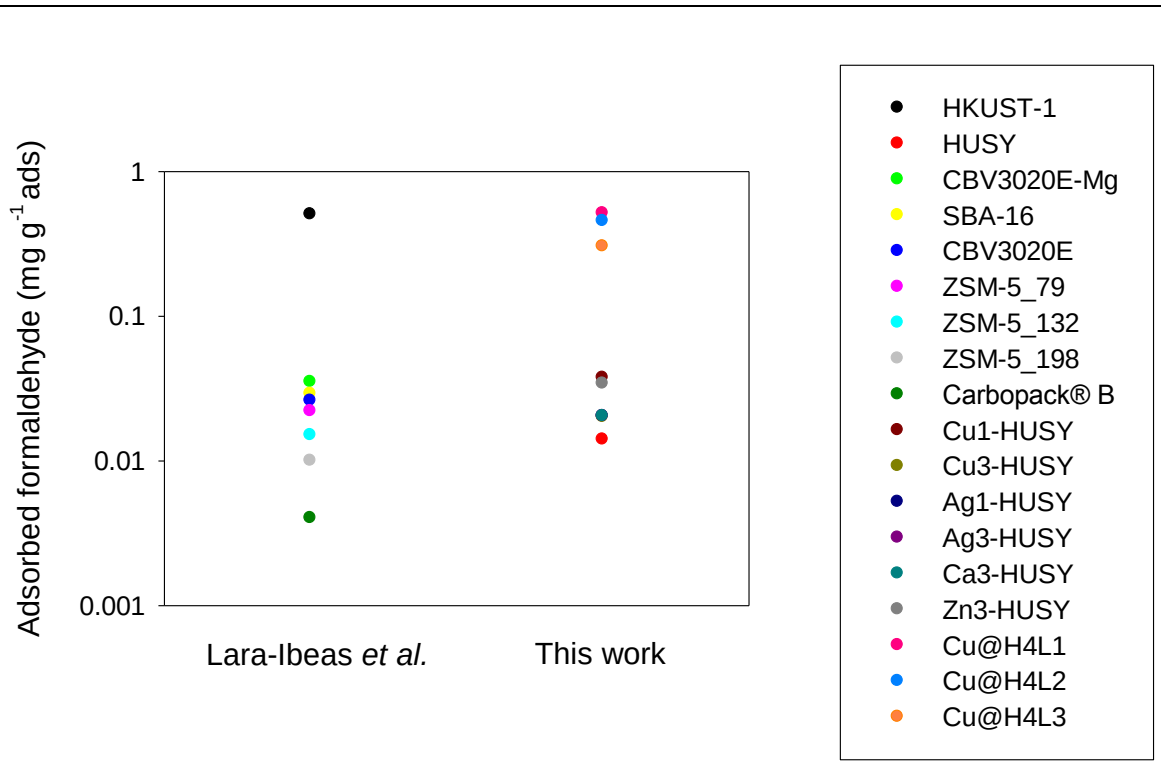

Figure 11. Formaldehyde adsorption capacities of diverse materials at a formaldehyde concentration of 0.164 ppm from the work of Lara-Ibeas *et al.* [56] and this work.

Thanks to the recent development of a new formaldehyde analyser operating in real time enabling adsorption experiments at realistic initial level of gaseous formaldehyde (164 ppb), it was possible to conduct adsorption measurements over different microporous materials. In these

experiments, the adsorption capacities of the microporous materials differing in structure, porosity and chemical composition were evaluated. Among them, SUM-102 material was demonstrated to be the more promising adsorbent for HCHO capture. Peculiar adsorbate-adsorbent repulsions between glyme or diglyme moieties and formaldehyde molecules were probably responsible for directing/hindering the diffusion of the latter molecules to reach the active sites. In addition, the side-chains present on SUM-102 and SUM-103 materials enhance the stability towards water/steam, thus allowing to avoid the integration of water-trapping devices when using them for formaldehyde removal applications. **Figure 11** demonstrates that Cu-based MOFs are more promising HCHO adsorbents than zeolites at least under realistic indoor conditions. Among the investigated MOFs, SUM-102 exhibited the highest surfacic adsorption capacity (0.52 $\mu g_{HCHO}\ m^{-2}$), yielding more than 1 kg_{HCHO} adsorbed per $m^3_{sorbent}$ being superior to the zeolite family by at least one order of magnitude.

Acknowledgments

This project has been supported by the European Union's through the LIFE SMART IN'AIR – Smart indoor air monitoring network to reduce the impacts of pollutants on environment and health – under grant number LIFE17 ENV/FR/000330. We express our gratitude to the French Ministry of Foreign Affairs for providing the PhD scholarship of NI.

References

[1] T. Salthammer, S. Mentese, R. Marutzky, Formaldehyde in the indoor environment, Chem Rev. 110 (2010) 2536–2572. https://doi.org/10.1021/cr800399g.

[2] N.L. Gilbert, M. Guay, D. Gauvin, R.N. Dietz, C.C. Chan, B. Lévesque, Air change rate and concentration of formaldehyde in residential indoor air, Atmospheric Environment. 10 (2008) 2424–2428. https://doi.org/10.1016/j.atmosenv.2007.12.017.

[3] C. Wang, X.-F. Huang, Y. Han, B. Zhu, L.-Y. He, Sources and Potential Photochemical Roles of Formaldehyde in an Urban Atmosphere in South China, Journal of Geophysical Research: Atmospheres. 122 (2017) 11,934-11,947. https://doi.org/10.1002/2017JD027266.

[4] T. Wangchuk, C. He, M. Dudzinska, L. Morawska, Seasonal variations of outdoor air pollution and factors driving them in the school environment in rural Bhutan, Atmospheric Environment. 113 (2015) 151–158. https://doi.org/10.1016/j.atmosenv.2015.05.004.

[5] B. Wang, S.C. Lee, K.F. Ho, Characteristics of carbonyls: Concentrations and source strengths for indoor and outdoor residential microenvironments in China, Atmospheric Environment. 41 (2007) 2851–2861. https://doi.org/10.1016/j.atmosenv.2006.11.039.

[6] S.-C. Lee, B. Wang, Characteristics of emissions of air pollutants from burning of incense in a large environmental chamber, Atmospheric Environment. 38 (2004) 941–951. https://doi.org/10.1016/j.atmosenv.2003.11.002.

[7] W. Xiaoyan, W. Huixiang, W. Shaoli, Ambient formaldehyde and its contributing factor to ozone and OH radical in a rural area, Atmospheric Environment. 44 (2010) 2074–2078. https://doi.org/10.1016/j.atmosenv.2010.03.023.

[8] T. Salthammer, The formaldehyde dilemma, International Journal of Hygiene and Environmental Health. 218 (2015) 433–436. https://doi.org/10.1016/j.ijheh.2015.02.005.

[9] M. Weng, L. Zhu, K. Yang, S. Chen, Levels, sources, and health risks of carbonyls in residential indoor air in Hangzhou, China, Environ Monit Assess. 163 (2010) 573–581. https://doi.org/10.1007/s10661-009-0859-z.

[10] C. Marchand, S. Le Calve, P. Mirabel, N. Glasser, A. Casset, N. Schneider, F. De Blay, Concentrations and determinants of gaseous aldehydes in 162 homes in Strasbourg (France), Atmospheric Environment. 42 (2008) 505–516.

[11] J.-Y. An, S. Kim, H.-J. Kim, Formaldehyde and TVOC emission behavior of laminate flooring by structure of laminate flooring and heating condition, Journal of Hazardous Materials. 187 (2011) 44–51. https://doi.org/10.1016/j.jhazmat.2010.08.086.

[12] C. Trocquet, I. Lara-Ibeas, A. Schulz, P. Bernhardt, B. Cormerais, S. Englaro, S. Le Calvé, Continuous aldehydes monitoring in primary schools in France: Evaluation of emission sources and ventilation practices over 5 weeks, Atmospheric Pollution Research. 12 (2021) 340–351. https://doi.org/10.1016/j.apr.2020.09.005.

[13] N.L. Gilbert, D. Gauvin, M. Guay, M.-È. Héroux, G. Dupuis, M. Legris, C.C. Chan, R.N. Dietz, B. Lévesque, Housing characteristics and indoor concentrations of nitrogen dioxide and formaldehyde in Quebec City, Canada, Environmental Research. 102 (2006) 1–8. https://doi.org/10.1016/j.envres.2006.02.007.

[14] L. Zhang, C. Steinmaus, D.A. Eastmond, X.K. Xin, M.T. Smith, Formaldehyde exposure and leukemia: A new meta-analysis and potential mechanisms, Mutation Research/Reviews in Mutation Research. 681 (2009) 150–168. https://doi.org/10.1016/j.mrrev.2008.07.002.

[15] C. Yrieix, A. Dulaurent, C. Laffargue, F. Maupetit, T. Pacary, E. Uhde, Characterization of VOC and formaldehyde emissions from a wood based panel: Results from an inter-laboratory comparison, Chemosphere. 79 (2010) 414–419. https://doi.org/10.1016/j.chemosphere.2010.01.062.

[16] P. Mamza, E. Ezeh, E. Gimba, D. Arthur, Comparative Study Of Phenol Formaldehyde And Urea Formaldehyde Particleboards From Wood Waste For Sustainable Environment, International Journal of Scientific & Technology Research. 3 (2014) 53–61.

[17] P. Solt, J. Konnerth, W. Gindl-Altmutter, W. Kantner, J. Moser, R. Mitter, H.W.G. van Herwijnen, Technological performance of formaldehyde-free adhesive alternatives for particleboard industry, International Journal of Adhesion and Adhesives. 94 (2019) 99–131. https://doi.org/10.1016/j.ijadhadh.2019.04.007.

[18] K.B. Rumchev, J.T. Spickett, M.K. Bulsara, M.R. Phillips, S.M. Stick, Domestic exposure to formaldehyde significantly increases the risk of asthma in young children, European Respiratory Journal. 20 (2002) 403–408. https://doi.org/10.1183/09031936.02.00245002.

[19] D. Poppendieck, H. Hubbard, M. Ward, C. Weschler, R.L. Corsi, Ozone reactions with indoor materials during building disinfection, Atmospheric Environment. 41 (2007) 3166–3176. https://doi.org/10.1016/j.atmosenv.2006.06.060.

[20] F. Rancière, C. Dassonville, C. Roda, A.-M. Laurent, Y. Le Moullec, I. Momas, Contribution of ozone to airborne aldehyde formation in Paris homes, Science of The Total Environment. 409 (2011) 4480–4483. https://doi.org/10.1016/j.scitotenv.2011.04.058.

[21] J. Williams, H. Li, A.B. Ross, S.P. Hargreaves, Quantification of the influence of NO2, NO and CO gases on the determination of formaldehyde and acetaldehyde using the DNPH method as applied to polluted environments, Atmospheric Environment. 218 (2019). https://eprints.whiterose.ac.uk/154288/ (accessed January 14, 2022).

[22] J.P. Porterfield, S. Eibenberger, D. Patterson, M.C. McCarthy, The ozonolysis of isoprene in a cryogenic buffer gas cell by high resolution microwave spectroscopy, Phys. Chem. Chem. Phys. 20 (2018) 16828–16834. https://doi.org/10.1039/C8CP02055H.

[23] M. Nicolas, O. Ramalho, F. Maupetit, Reactions between ozone and building products: Impact on primary and secondary emissions, Atmospheric Environment. 41 (2007) 3129–3138. https://doi.org/10.1016/j.atmosenv.2006.06.062.

[24] Décret n° 2011-1727 du 2 décembre 2011 relatif aux valeurs-guides pour l'air intérieur pour le formaldéhyde et le benzène, 2011.

[25] A. Casset, A. Purohit, C. Marchand, S. Le Calvé, C. Donnay, B. Uring-Lambert, S. Bahram, G. Pauli, F. de Blay, The bronchial response to inhaled formaldehyde, Rev Mal Respir. 23 (2006) 3S25-34.

[26] X. Tang, Y. Bai, A. Duong, M. Smith, L. Li, L. Zhang, Formaldehyde in China: Production, consumption, exposure levels, and health effects, Environment International. 36 (2009) 1210–1224. https://doi.org/10.1016/j.envint.2009.06.002.

[27] G. McGwin, J. Lienert, J.I. Kennedy, Formaldehyde Exposure and Asthma in Children: A Systematic Review, Environ Health Perspect. 118 (2010) 313–317. https://doi.org/10.1289/ehp.0901143.

[28] S. Suresh, T.J. Bandosz, Removal of formaldehyde on carbon -based materials: A review of the recent approaches and findings, Carbon. 137 (2018) 207–221. https://doi.org/10.1016/j.carbon.2018.05.023.

[29] C. Trocquet, P. Bernhardt, M. Guglielmino, I. Malandain, C. Liaud, S. Englaro, S. Le Calvé, Near Real-Time Monitoring of Formaldehyde in a Low-Energy School Building, Atmosphere. 10 (2019) 763. https://doi.org/10.3390/atmos10120763.

[30] A. Allouch, M. Guglielmino, P. Bernhardt, C.A. Serra, S. Le Calvé, Transportable, fast and high sensitive near real-time analyzers: Formaldehyde detection, Sensors and Actuators B: Chemical. 181 (2013) 551–558. https://doi.org/10.1016/j.snb.2013.02.043.

[31] M. Guglielmino, P. Bernhardt, C. Trocquet, C.A. Serra, S. Le Calvé, On-line gaseous formaldehyde detection by a microfluidic analytical method based on simultaneous uptake and derivatization in a temperature controlled annular flow, Talanta. 172 (2017) 102–108. https://doi.org/10.1016/j.talanta.2017.05.038.

[32] B. Hanoune, T. LeBris, L. Allou, C. Marchand, S. Le Calvé, Formaldehyde measurements in libraries: Comparison between infrared diode laser spectroscopy and a DNPH-derivatization method, Atmospheric Environment. 40 (2006) 5768–5775. https://doi.org/10.1016/j.atmosenv.2006.05.017.

[33] A. Becker, C. Andrikopoulou, P. Bernhardt, R. Ocampo-Torres, C. Trocquet, S. Le Calvé, Development and Optimization of an Airborne Formaldehyde Microfluidic Analytical Device Based on Passive Uptake through a Microporous Tube, Micromachines. 10 (2019) 807. https://doi.org/10.3390/mi10120807.

[34] A. Becker, C. Andrikopoulou, P. Bernhardt, R. OCAMPO-TORRES, C. Trocquet, S. Le Calvé, On-Line Gaseous Formaldehyde Detection Based on a Closed-Microfluidic-Circuit Analysis, Chemosensors. 8 (2020) 57. https://doi.org/10.3390/chemosensors8030057.

[35] S. Le Calvé, C. Andrikopoulou, A. Becker, C. Trocquet, H. Plaisance, FR3097967 Procédé et dispositifs d'analyses microfluidiques pour la quantification de polluants gazeux solubles dans l'eau, (2021). https://patentscope.wipo.int/search/fr/detail.jsf?docId=FR315301918&_cid=P10-KSQ19R-92862-1 (accessed February 5, 2022).

[36] D. Mariuta, A. Govindaraji, S. Colin, C. Barrot, S. Le Calvé, J.G. Korvink, L. Baldas, J.J. Brandner, Optofluidic Formaldehyde Sensing: Towards On-Chip Integration, Micromachines. 11 (2020) 673. https://doi.org/10.3390/mi11070673.

[37] J. van den Broek, D.K. Cerrejon, A.T. Guntner, S.E. Pratsinis, Compact Formaldehyde Detector Based on Filter–Sensor System with Validated Performance in Indoor Air, Meet. Abstr. MA2021-01 (2021) 1567. https://doi.org/10.1149/MA2021-01581567mtgabs.

[38] C. Liao, M. Zhang, N. Gao, Q. Tian, J. Shi, S. Chen, C. Wang, L. Zang, Paper-Based Vapor Detection of Formaldehyde: Colorimetric Sensing with High Sensitivity, Chemosensors. 9 (2021) 335. https://doi.org/10.3390/chemosensors9120335.

[39] D. Mariuta, L. Baldas, S. Colin, S. Le Calvé, J.G.G. Korvink, J.J. Brandner, Prototyping a miniaturized microfluidic sensor for real-time detection of airborne formaldehyde, International Journal of Chemical Engineering and Applications. 11 (2020) 23–28. https://doi.org/10.18178/ijcea.2020.11.1.774.

[40] L. Feng, L. Feng, Q. Li, J. Cui, J. Guo, Sensitive Formaldehyde Detection with QCM Sensor Based on PAAm/MWCNTs and PVAm/MWCNTs, ACS Omega. 6 (2021) 14004–14014. https://doi.org/10.1021/acsomega.0c05987.

[41] Y.K. Jo, S.-Y. Jeong, Y.K. Moon, Y.-M. Jo, J.-W. Yoon, J.-H. Lee, Exclusive and ultrasensitive detection of formaldehyde at room temperature using a flexible and monolithic chemiresistive sensor, Nat Commun. 12 (2021) 4955. https://doi.org/10.1038/s41467-021-25290-3.

[42] A. Baldelli, M. Jeronimo, M. Tinney, K. Bartlett, Real-time measurements of formaldehyde emissions in a gross anatomy laboratory, SN Appl. Sci. 2 (2020) 769. https://doi.org/10.1007/s42452-020-2569-7.

[43] H. Zhang, R. Srinivasan, V. Ganesan, Low Cost, Multi-Pollutant Sensing System Using Raspberry Pi for Indoor Air Quality Monitoring, Sustainability. 13 (2021) 370. https://doi.org/10.3390/su13010370.

[44] H. Zhang, R. Srinivasan, A Systematic Review of Air Quality Sensors, Guidelines, and Measurement Studies for Indoor Air Quality Management, Sustainability. 12 (2020) 9045. https://doi.org/10.3390/su12219045.

[45] K.E. Noll, Adsorption Technology for Air and Water Pollution Control, CRC Press, 1991.

[46] W.M.T.M. Reimerink, D. v. d Kleut, Air pollution control by adsorption, Studies in Surface Science and Catalysis. 120 (1999) 807–819. https://doi.org/10.1016/S0167-2991(99)80380-2.

[47] X. Yue, N.L. Ma, C. Sonne, R. Guan, S.S. Lam, Q. Van Le, X. Chen, Y. Yang, H. Gu, J. Rinklebe, W. Peng, Mitigation of indoor air pollution: A review of recent advances in adsorption materials and catalytic oxidation, Journal of Hazardous Materials. 405 (2021) 124138. https://doi.org/10.1016/j.jhazmat.2020.124138.

[48] ISO 16000-3:2011 Indoor air - Part 3: Determination of formaldehyde and other carbonyl compounds - Active sampling method, (2011).

[49] M. Guglielmino, A. Allouch, C.A. Serra, S.L. Calvé, Development of microfluidic analytical method for on-line gaseous Formaldehyde detection, Sensors and Actuators B: Chemical. 243 (2017) 963–970. https://doi.org/10.1016/j.snb.2016.11.093.

[50] J.-P. Bellat, I. Bezverkhyy, G. Weber, S. Royer, R. Averlant, J.-M. Giraudon, J.-F. Lamonier, Capture of formaldehyde by adsorption on nanoporous materials, Journal of Hazardous Materials. 300 (2015) 711–717. https://doi.org/10.1016/j.jhazmat.2015.07.078.

[51] E.M. Carter, L.E. Katz, G.E. Speitel, D. Ramirez, Gas-Phase Formaldehyde Adsorption Isotherm Studies on Activated Carbon: Correlations of Adsorption Capacity to Surface Functional Group Density, Environ. Sci. Technol. 45 (2011) 6498–6503. https://doi.org/10.1021/es104286d.

[52] A. Kalantarifard, J.G. Gon, G.S. Yang, Formaldehyde Adsorption into Clinoptilolite Zeolite Modified with the Addition of Rich Materials and Desorption Performance Using Microwave Heating, in: 2016. https://doi.org/10.3319/tao.2016.05.28.01(tt).

[53] A. Nomura, C.W. Jones, Amine-Functionalized Porous Silicas as Adsorbents for Aldehyde Abatement, ACS Appl. Mater. Interfaces. 5 (2013) 5569–5577. https://doi.org/10.1021/am400810s.

[54] Z. Wang, W. Wang, D. Jiang, L. Zhang, Y. Zheng, Diamine-appended metal–organic frameworks: enhanced formaldehyde-vapor adsorption capacity, superior recyclability and water resistibility, Dalton Trans. 45 (2016) 11306–11311. https://doi.org/10.1039/C6DT01696K.

[55] Z. Zhao, S. Wang, Y. Yang, X. Li, J. Li, Z. Li, Competitive adsorption and selectivity of benzene and water vapor on the microporous metal organic frameworks (HKUST-1), Chemical Engineering Journal. 259 (2015) 79–89. https://doi.org/10.1016/j.cej.2014.08.012.

[56] I. Lara-Ibeas, C. Megías-Sayago, B. Louis, S. Le Calvé, Adsorptive removal of gaseous formaldehyde at realistic concentrations, Journal of Environmental Chemical Engineering. 8 (2020) 103986. https://doi.org/10.1016/j.jece.2020.103986.

[57] C. Megías-Sayago, I. Lara-Ibeas, Q. Wang, S. Le Calvé, B. Louis, Volatile organic compounds (VOCs) removal capacity of ZSM-5 zeolite adsorbents for near real-time BTEX detection, Journal of Environmental Chemical Engineering. 8 (2020) 103724. https://doi.org/10.1016/j.jece.2020.103724.

[58] S. Dong, Dasgupta, Solubility of gaseous formaldehyde in liquid water and generation of trace standard gaseous formaldehyde, Environ. Sci. Technol. 20 (1986) 637–640. https://doi.org/10.1021/es00148a016.

[59] F.F. Andrawes, Detection of Traces of Formaldehyde in Pure Air by Gas Chromatography and Helium Ionization Detection, Journal of Chromatographic Science. 22 (1984) 506–508. https://doi.org/10.1093/chromsci/22.11.506.

[60] R. Aoyagi, K. Matsunobu, Stability of Formaldehyde Calibration Gas by Permeation Tube Using Paraformaldehyde, Indoor Environment. 15 (2012) 7–14. https://doi.org/10.7879/siej.15.7.

[61] A. Becker, N. Lohmann, C.A. Serra, S. Le Calvé, Development of a Portable and Modular Gas Generator: Application to Formaldehyde Analysis, Chemosensors. 10 (2022) 131. https://doi.org/10.3390/chemosensors10040131.

[62] J. Luong, X. Yang, Y. Hua, P. Yang, R. Gras, Gas Chromatography with In Situ Catalytic Hydrogenolysis and Flame Ionization Detection for the Direct Measurement of Formaldehyde and Acetaldehyde in Challenging Matrices, Anal. Chem. 90 (2018) 13855–13859. https://doi.org/10.1021/acs.analchem.8b04563.

[63] H. Zhu, J. She, M. Zhou, X. Fan, Rapid and sensitive detection of formaldehyde using portable 2-dimensional gas chromatography equipped with photoionization detectors, Sensors and Actuators B: Chemical. 283 (2019) 182–187. https://doi.org/10.1016/j.snb.2018.11.156.

[64] A. Kapoor, R.T. Yang, Correlation of equilibrium adsorption data of condensible vapours on porous adsorbents, Gas Separation & Purification. 3 (1989) 187–192. https://doi.org/10.1016/0950-4214(89)80004-0.

[65] G. Sposito, On the Use of the Langmuir Equation in the Interpretation of "Adsorption" Phenomena: II. The "Two-Surface" Langmuir Equation, Soil Science Society of America Journal. 46 (1982) 1147–1152. https://doi.org/10.2136/sssaj1982.03615995004600060006x.

[66] A.J. Maia, B. Louis, Y.L. Lam, M.M. Pereira, Ni-ZSM-5 catalysts: Detailed characterization of metal sites for proper catalyst design, Journal of Catalysis. 269 (2010) 103–109. https://doi.org/10.1016/j.jcat.2009.10.021.

[67] N. Israfilov, K. Soukup, B. Louis, J.-M. Planeix, MOF side chains as sources of supramolecular interactions: organic pollutant extraction from water, New Journal of Chemistry 46 (2022) 8967-8970. https://doi.org/10.1039/D2NJ00273F.

[68] H.-M. Wen, G. Chang, B. Li, R.-B. Lin, T.-L. Hu, W. Zhou, B. Chen, Highly Enhanced Gas Uptake and Selectivity via Incorporating Methoxy Groups into a Microporous Metal–Organic Framework, Crystal Growth & Design. 17 (2017) 2172–2177. https://doi.org/10.1021/acs.cgd.7b00111.

[69] M. Guglielmino, A. Allouch, C.A. Serra, S.L. Calvé, Development of microfluidic analytical method for on-line gaseous Formaldehyde detection, Sensors and Actuators B: Chemical. 243 (2017) 963–970. https://doi.org/10.1016/j.snb.2016.11.093.

[70] C. Trocquet, P. Bernhardt, M. Guglielmino, I. Malandain, C. Liaud, S. Englaro, S. Le Calvé, Near Real-Time Monitoring of Formaldehyde in a Low-Energy School Building, Atmosphere. 10 (2019). https://doi.org/10.3390/atmos10120763.

[71] U. Eisner, J. Kuthan, Chemistry of dihydropyridines, Chemical Reviews. 72 (1972) 1–42. https://doi.org/10.1021/CR60275A001.

[72] X. Lin, I. Telepeni, A.J. Blake, A. Dailly, C.M. Brown, J.M. Simmons, M. Zoppi, G.S. Walker, K.M. Thomas, T.J. Mays, P. Hubberstey, N.R. Champness, M. Schröder, High Capacity Hydrogen Adsorption in Cu(II) Tetracarboxylate Framework Materials: The Role of Pore Size, Ligand Functionalization, and Exposed Metal Sites, J. Am. Chem. Soc. 131 (2009) 2159–2171. https://doi.org/10.1021/ja806624j.

[73] R.P. Townsend, E.N. Coker, Chapter 11 Ion exchange in zeolites, in: H. van Bekkum, E.M. Flanigen, P.A. Jacobs, J.C. Jansen (Eds.), Studies in Surface Science and Catalysis, Elsevier, 2001: pp. 467–524. https://doi.org/10.1016/S0167-2991(01)80253-6.

[74] S. Kulprathipanja, Zeolites in Industrial Separation and Catalysis, John Wiley & Sons, 2010.

[75] E. Kukulska-Zając, J. Datka, Transformations of Formaldehyde Molecules in Cu−ZSM-5 Zeolites, J. Phys. Chem. C. 111 (2007) 3471–3475. https://doi.org/10.1021/jp066732g.

[76] J.-P. Bellat, G. Weber, I. Bezverkhyy, J.-F. Lamonier, Selective adsorption of formaldehyde and water vapors in NaY and NaX zeolites, Microporous and Mesoporous Materials. 288 (2019) 109563. https://doi.org/10.1016/j.micromeso.2019.109563.

[77] R.G. Pearson, Hard and Soft Acids and Bases, ACS Publications. (1963). https://doi.org/10.1021/ja00905a001.

[78] T.-L. Ho, Hard soft acids bases (HSAB) principle and organic chemistry, ACS Publications. (2002). https://doi.org/10.1021/cr60293a001.

[79] P. Costa, V. Ferreira, P. Esteves, M. Vasconcellos, Ácidos e bases em química orgânica, Ed. Bookmann, Porto Alegre, RS. (2005).

[80] P.D. Kleiber, W. Lu, Y. Abate, Spectroscopy and chemical dynamics of group II metal ion-formaldehyde complexes, International Journal of Mass Spectrometry. 269 (2008) 1–11. https://doi.org/10.1016/j.ijms.2007.09.002.

[81] T. Dutta, K.-H. Kim, R.J.C. Brown, Y.-H. Kim, D. Boukhvalov, Metal-organic framework and Tenax-TA as optimal sorbent mixture for concurrent GC-MS analysis of C1 to C5 carbonyl compounds, Sci Rep. 8 (2018) 5033. https://doi.org/10.1038/s41598-018-23391-6.

[82] P. Küsgens, M. Rose, I. Senkovska, H. Fröde, A. Henschel, S. Siegle, S. Kaskel, Characterization of metal-organic frameworks by water adsorption, Microporous and

Mesoporous Materials. 120 (2009) 325–330. https://doi.org/10.1016/j.micromeso.2008.11.020.

[83] E. Ahmed, A. Deep, E.E. Kwon, R.J.C. Brown, K.-H. Kim, Performance comparison of MOF and other sorbent materials in removing key odorants emitted from pigpen slurry, Sci Rep. 6 (2016) 31283. https://doi.org/10.1038/srep31283.

[84] C.-J. Na, M.-J. Yoo, D.C.W. Tsang, H.W. Kim, K.-H. Kim, High-performance materials for effective sorptive removal of formaldehyde in air, Journal of Hazardous Materials. 366 (2019) 452–465. https://doi.org/10.1016/j.jhazmat.2018.12.011.

[85] J.E. Szulejko, K.-H. Kim, J. Parise, Seeking the most powerful and practical real-world sorbents for gaseous benzene as a representative volatile organic compound based on performance metrics, Separation and Purification Technology. 212 (2019) 980–985. https://doi.org/10.1016/j.seppur.2018.11.001.

[86] K. Vellingiri, P. Kumar, A. Deep, K.-H. Kim, Metal-organic frameworks for the adsorption of gaseous toluene under ambient temperature and pressure, Chemical Engineering Journal. 307 (2017) 1116–1126. https://doi.org/10.1016/j.cej.2016.09.012.

[87] D.P. Serrano, G. Calleja, J.A. Botas, F.J. Gutierrez, Characterization of adsorptive and hydrophobic properties of silicalite-1, ZSM-5, TS-1 and Beta zeolites by TPD techniques, Separation and Purification Technology. 54 (2007) 1–9. https://doi.org/10.1016/j.seppur.2006.08.013.

[88] C. Fu, T. Chen, T. Xiao, Y. Song, T. Odom, W. Liang, J. Cai, H. Xu, Formaldehyde Gas Adsorption in High-Capacity Silver-Nanoparticle-Loaded ZIF-8 and UiO-66 Frameworks, ChemistrySelect. 5 (2020) 5987–5992. https://doi.org/10.1002/slct.202001094.

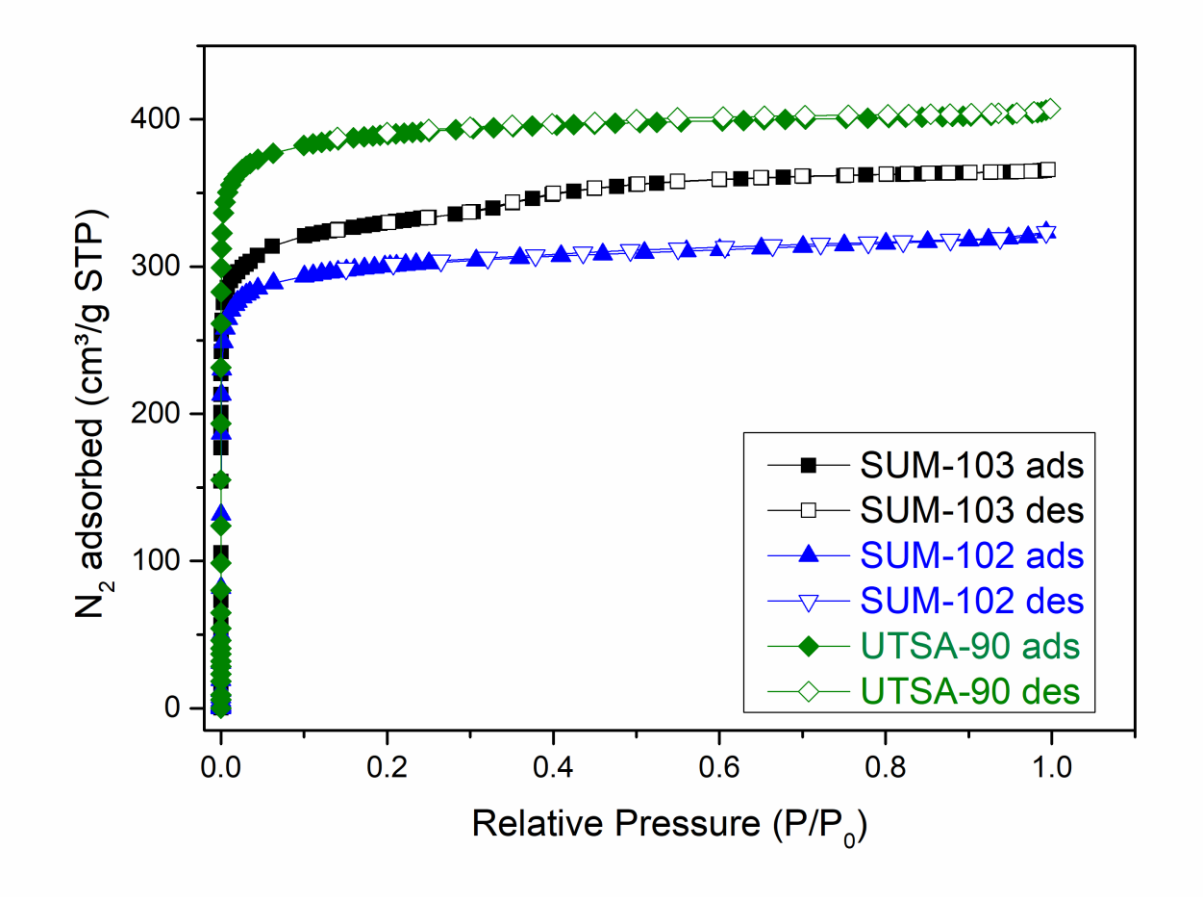

Figure S1. N_2 adsorption-desorption isotherms for home-made Cu-MOFs